Original scientific paper

INFLUENCE OF CROSSING WEAR ON ROLLING CONTACT FATIGUE DAMAGE OF FROG RAIL

Lei Kou[1], Mykola Sysyn[1], Jianxing Liu[2]

[1]Institute of Railway Systems and Public Transport, TU-Dresden, Germany
[2]School of Civil Engineering, Southwest Jiaotong University, Chengdu, China

ORCID iDs: Lei Kou   https://orcid.org/0000-0001-5372-6305
           Mykola Sysyn   https://orcid.org/0000-0001-6893-0018
           Jianxing Liu   https://orcid.org/0000-0002-4779-7761

Abstract. *The damage of the frog rail significantly affects the wear of the crossing rail and restricts the passing speed of the train. A geometric 3D modeling of the vehicle passing through the crossing center is particularly concerned with the cumulative wheel-rail contact of the traffic volume. The frog rail wear is simulated to obtain the dynamic change of the impact force of the wheel on the frog rail as the rail wears. By summarizing the existing experimental results of other scholars, it is clear that the important factors, that cause the damage of the frog rail, are vehicle load, friction coefficient, slip roll ratio and shear stress. This paper combines the theoretical analysis of mechanics and 3D simulation to obtain the position change of the wheel-rail contact point with the wear of the frog rail, and finally compares it with the actual measurement results. It can more accurately predict the area where the maximum damage occurs after a certain amount of traffic for a certain fixed model, the change of wheel-rail contact point at frog rail is simulated with the wear of each component. Through theoretical analysis, the main factors determining frog rail damage were determined. Then evaluate the possible damage area of the frog track and control the prediction range to 5-10 cm, which reduces the detection time and cost. The worst state of distraction will be detected in time to facilitate replacement or polishing. Through further research in this area, the service life of the frog rail can be predicted.*

Key words: *Railway crossing, RCF, Wheel-rail contact, Rail surface defect, Frog wear, Geometric model*

1. INTRODUCTION

Since the birth of the railway, one of the main problems faced by the railway is rail failure. As with all high-speed driving modes, the failure of necessary components can have serious consequences. Railway companies around the world have been inspecting their most expensive infrastructure assets. The increase in freight rail traffic and the increase in speed have made railway inspections today more important than ever. Railway superstructures need to resist a relatively high load due to the more vehicles running on them [1]. Although the focus of the inspection seems to be a well-defined piece of steel, the presence of test variables is important and makes the inspection process challenging. Crossing is a general term for the connection and crossing device between railroad rolling stocks that transfer from one track to another. This device is called special track work in railway engineering. The crossing conversion system is an important crossing device for the railway to change the track, which directly affects the safety of the train. The increase failure rate in crossing device will affect operational efficiency. Therefore, it is urgent and necessary to monitor the status of crossing device, diagnose and predict failures. The crossing can be divided into three units: crossing (or checkrail), frog (or crossing center) and its connecting part (closure panel). Switches and crossings are the essential elements of railway lines, allowing a change in direction, or the transfer of a vehicle from one track to another [2]. In the life of the rail system, the fatigue sensitive positions of the track structure in the crossing area are frog, spring bar and track plate. The frog rail is an important part of the system. Its structure is relatively weak, but it has to withstand a huge impact when the train changes direction, and there is a "harmful space" at the frog rail of the crossing, which endangers driving safety. Risk management plays a key role in railway projects [3]. Therefore, it needs to be inspected and maintained regularly to ensure the safety of train operation.

Many scholars have conducted research on rail damage detection. Traditional rail surface detection uses manual inspection, which is inefficient, and the accuracy of detection results fluctuates widely. In order to improve the detection efficiency and obtain standardized detection results, methods such as geometric measurement [4], ultrasonic testing [5], eddy current testing [6], and rail surface defect detection based on machine vision [7, 8] have been successively developed around the world. So far, the research on frog rail is relatively limited, and the changing cross-sectional shape of the frog rail of the crossing has brought a great challenge to the accuracy of detection. For the detection of the frog rail, it is usually necessary to obtain the data of the entire area. The data can only be completed manually. In actual operation, complete collection is not only dangerous, but also takes a lot of time. Determining the representative damage area of the frog rail and reducing it to a certain range can reduce the detection time and cost, and the accuracy of the preliminary data can improve the accuracy of computer vision detection. Only by understanding the changes in the mechanical characteristics between worn wheels and rails and determining the location of the largest damaged area, we can accurately optimize the geometry of the crossing, improve the optimization efficiency, and improve the speed and safety of the train passing the crossing. The further research on the damage generation process is of great significance.

In the crossing area, because the rolling direction of the entering wheel is different from the guiding direction of the frog rail, the decay speed of the longitudinal wheel-rail force is greater than the decay speed of the vertical wheel-rail force. The geometric incompatibility of the crossing during the collision will aggravate the tangential wheel-rail collision, and

the slip area in the wheel-rail contact surface will be significantly enlarged at this time [9]. The articles [10-14] studied wheel-rail contact through geometric modeling, mechanical model analysis of stress distribution, and actual measurement of wheel-rail vibration, and studied the optimal design of the geometry or loading of the crossing in its core rail. The article [15] collects the profile of wheel tread change during the entire life cycle of the wheel and establishes the dynamic model when the wheel passes through the fixed frog rail, which proves that the wheel wear is beneficial to alleviate the damage of the frog rail. The article [16] carried out a numerical simulation of the contact stress between the core rail and the wheel and determined the most important reason for the rapid wear of the frog rail. Mykola Sysyn et al.'s research on the crack generation process of the frog rail of the crossing gives a lot of inspiration [17] and the statistical analysis of the three-axis acceleration of the frog rail due to the effect of the rail when the train passes the core rail [18]. The study found that the maximum damage area of the frog rail is not necessarily related to the impact distribution of the frog rail. Machine learning shows that the damage of the frog rail is only related to a small part of the high-impact with wheel-rail effects. In this article, a three-dimensional geometric model is first established to simulate the evolution of the frog rail's contact with the wheel as the amount of wear increases, and to determine the important area of wheel-rail contact. Afterwards, through analysis and summary, the main factors affecting the wear of frog rail are found, and the most important influencing factors are obtained through theoretical comparison. Then we explore the location of important influencing factors, determine the area where the largest damage occurs in the life cycle of the frog rail, and finally compare the results with the actual collected location data of the frog rail damage to obtain the theoretical and actual double inspection results.

2. GEOMETRIC MODEL

2.1. Basis data

Due to the presence of variable cross-section rails at the frog rail, it is difficult to establish a three-dimensional model. The irregularity of the cross-section shape change of the frog rail is one of the important features of the frog rail model. This feature makes the wheel-rail contact characteristics of the crossing area comparable to the general line. There is a fundamental difference. The crossing modeled here is a crossing with an intersection angle of 1:12. We use the unworn wheel profile first. In the paper [19], L. Xin et al. showed a universally applicable cross-section data of frog rail to construct a frog track geometric model. The cross nose in the model is constructed using four main cross sections, which are defined by drawings provided by the manufacturer (Fig. 1). The distances between the four cross-sections in the figure are 10a, 10a, and 50a, and the unit here is uniformly millimeters. In addition "a" is equal to the intersection angle of the crossing (the crossing in this article is 1:12, so a = 12). The geometric parameters of the wheel tread in Fig. 2 are from the paper [20] and are the external dimensions of the LM tread in China, as shown on the left in Figure 2. Its characteristics: the width of the wheel flange is 32 mm and the height is 27 mm. The inner side of the rim has a guide angle to guide the wheel through the guardrail smoothly. The rail profile is based on the 60 kg/m rail cross section data in accordance with the Chinese standard GB2585-2007.
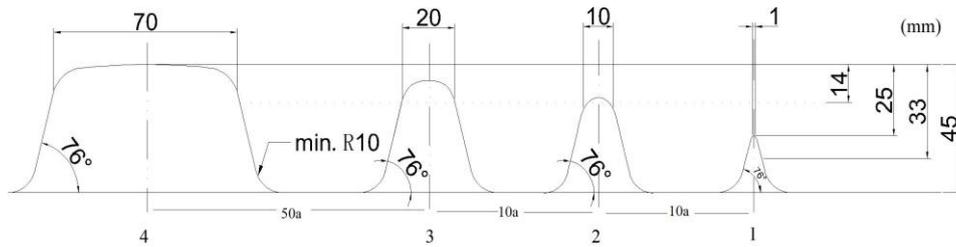
Fig. 1 Section drawing from the manufacturer
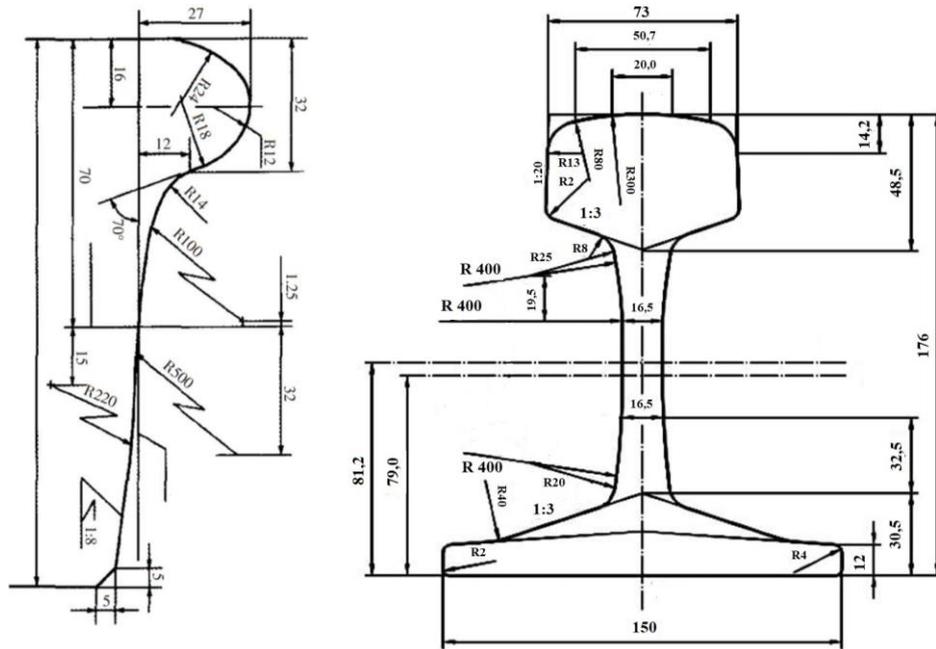

Fig. 2 Wheel tread and rail section

2.2. Model building

The main method to deal with the characteristics of variable section of rail is to calculate the whole variable section of rail by interpolation. Four control sections of frog track with variable cross section of crossing are given in the standard drawing. According to these standard sections, the profile of any section can be obtained by linear interpolation. The wheel and wing rail only need to extend in their direction. Here, because only the outline of the rail head is needed to participate in the calculation, the basic rail section in Fig. 2 is selected for the wing rail, and the distance between it and the cross section of the heart rail remains 44 mm with the extension of the direction. MATLAB interpolation calculation can be obtained along the direction of the train every 0.5 mm interpolation and horizontal every 0.05 mm geometric interpolation. Thus, a complete geometric model of the wheel passing through the center rail is obtained (Fig. 3).
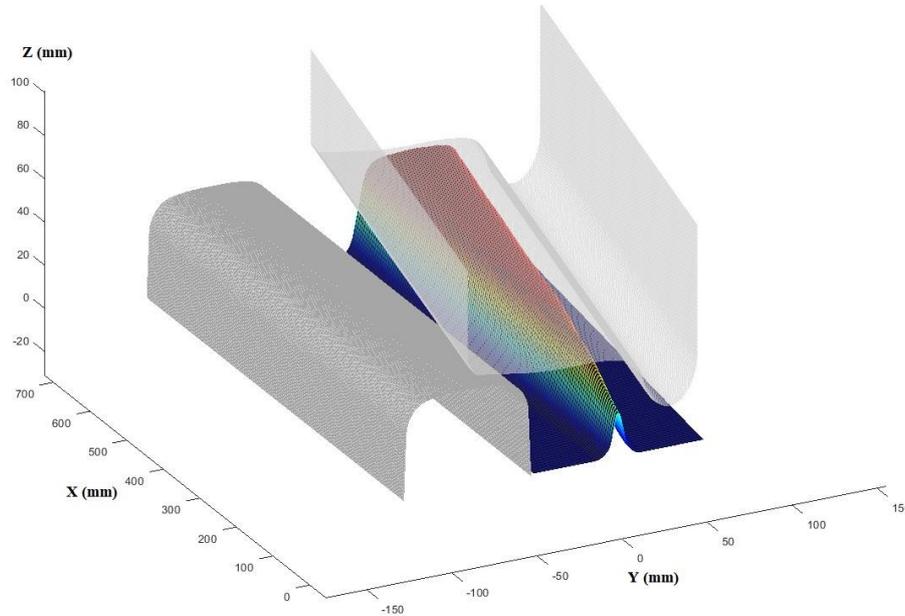
Fig. 3 Geometric 3D Model

Among the existing studies, the research direction of the paper [20, 21] is mainly focused on the influence of the wear of the frog rail on the interaction relationship between the wheel and crossing rail. It is concluded that the inner rail of the transition range of wheel load is impacted by wheel load due to the harmful space of the fixed frog, and the frog rail's top width of 20 ~ 40 mm is the area with larger vertical wear. The wheel-load transition area is very short, and the wheel-rail impact square is used to complete the wheel-load transition. As the vertical grinding of frog rail increases, the collision point between wheel and frog rail is far away from the theoretical tip, and the contact force fluctuation increases before and after the wheel load transition, the contact force peak increases, and the wheel load transition becomes unstable. In terms of [15] and [22], the research direction is mainly focused on the influence of wheel wear on the interaction relationship between a wheel and crossing rail. It was determined that RCF had the highest risk in the crown of frog rail and that contour wear reduced the dynamic response. The above studies have determined that rail wear at different levels and wheel wear have a significant impact on the overturning wheel-rail contact state because they affect stress and strain states. In this study, it is necessary to consider the wheel-rail contact state under the combination of frog rail wear, wheel wear and wing rail wear. As shown in Fig. 4 (a), contour calculation of three wear stages was carried out for the three components according to the wear state in the. Fig. 4 (b) shows how to judge the contact point method. If *D1* is greater than *D2*, the wheel is in contact with the wing rail; otherwise, it is in contact with the frog rail. We can set the threshold for simultaneous contact. The contact point between wheel and rail can be obtained according to the method on the right side of Fig. 4(c). Since the surface damage of frog rail is studied in this paper, the points that contact with the side of frog rail at the same time are not specifically calculated.
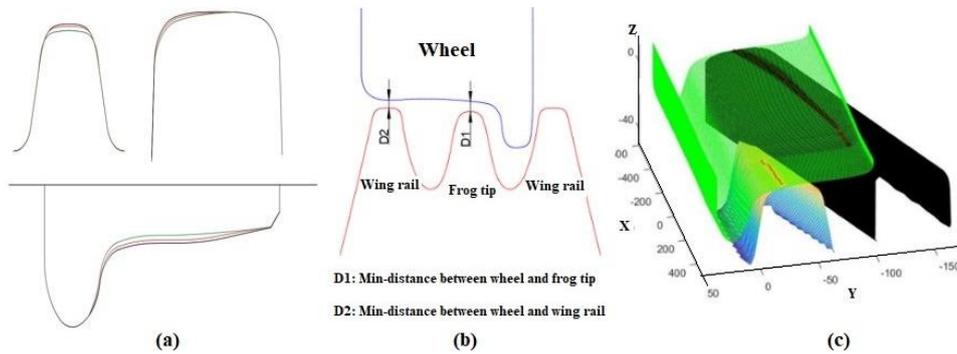
Fig. 4 Wear simulation of three components and model

3. ANALYSIS OF FROG DAMAGE

The model significantly shows the contact area when the wheel passes the crossing. Taking the 1:12 crossing as an example, the interval of 180 mm - 450 mm belongs to the transition area, in which a section of wheels can act on the frog rail and wing rail at the same time. When the load increases and the wheel-rail contact stress exceeds the yield limit of the bifurcated material, the material will undergo plastic deformation. Under the action of repeated loading, the plastic deformation will accumulate and increase, forming microscopic cracks on the surface and sub-surface of the material. Under the action of larger normal and tangential stresses, the microscopic cracks will expand and form fish-scale cracks distributed on the surface of the rail, that is, the phenomenon of "cracking". If the surface of frog rail cracks is not dealt with in time, the surface cracks will spread to the frog rail body along the direction of movement, and then large pieces of peeling. Rail stripping is mainly caused by the action of surface friction. With the increase of friction, the peeling phenomenon of material surface increases and the peeling chip block increases. Therefore, this area is also the most prone to damage of frog rail, and the wear coefficient will be affected by load, tangential force, sliding speed and initial surface state. In the process of changing from running-in wear stage to stable wear stage, the wear coefficient of texture surface and grinding polished surface gradually approach. In order to determine the damaged area more accurately, theoretical analysis of the interaction through the frog rail is essential.

3.1. The dynamic interaction in the common crossing

The dynamic interaction in the common crossing results from the constructive and wear geometrical properties. Wheel tread is not horizontal, but inclined. When the wheel travels through the crossing, the geometric locations of the contact points (between wheel and wing rail or between wheel and crossing nose) form a line [23]. This line is the wheel trajectory during the traveling and called constructive stimulation. The deviation of the wing rail creates a relative displacement between the wheel and the wing rail in the direction from wings rail to frog. Then there is a vertical wheel sink ΔZ [24]. Because of the surface inclination of the frog tip on Fig. 2, the wheel set rises after the touchdown point. The trends of rise and descent are reserved in the stump-travel. The length caused by

the increase and decrease is called the wavelength λ. The depth of the wheel descent is shown as amplitude of stimulation Z_S [25].

According to Fig. 5, it is determined that the geometrically exact stimulation is asymmetrical. The steeper rise with stump travel means that the load on the crossing is higher than with tip travel. Since both directions of travel occur, a reduction of the considerations on stump-travel is on the safe side. Then we design the wheel trajectory is simplified into a symmetrical shape, as shown in Fig. 5.
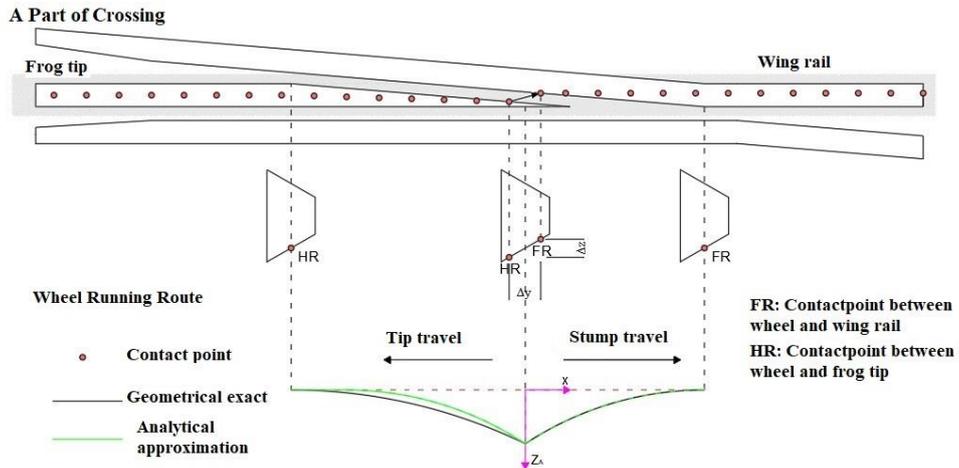
Fig. 5 The contact process analysis of the vibration system wheel-rail

The stimulation is described by two curves (Fig. 6), which show a clear transition at the connection point in the pass-through area. When the wheel passes through this area, one should analyze stimulation models. On the one hand, a wave-shaped stimulation in contact area with the wavelength λ and the wave depth Z_S (soft wave stimulation) is generated on the
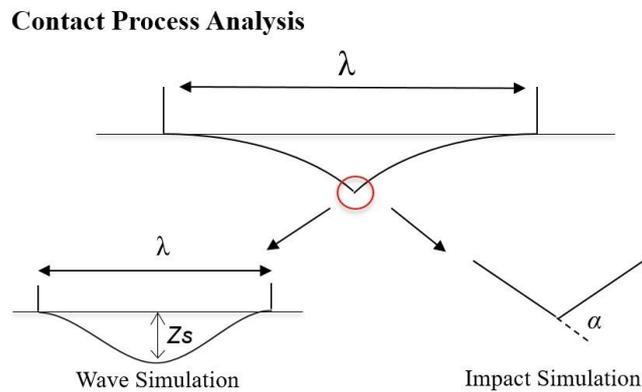
Fig. 6 Contact process analysis

other hand there is an impact by the transition (hard impact stimulation) with an angle α. Where the impact stimulation happened is the touchdown point and the angle α is touchdown angle [26]. Soft wave and hard impact are the two macroscopic effects of wheel-rail contact on the frog rail area of the crossing, and they are important reasons for the wear of the frog rail.

3.2. Factors of rail failure

Steel under the action of alternating stress, the stress is far lower than the tensile strength of static load, even when the yield strength of static load is lower than the sudden failure, this failure is called fatigue failure. The damage to rail caused by wheel rolling over rail is also fatigue damage. Analysis of all rolling contact processes shows that the front of the contact point between the wheel and track is in a state of compressive stress and its rear and secondary surfaces are in a state of tensile stress. The tangential plastic deformation of rail is caused by wheel friction, and the deformation accumulates gradually with the increase of cyclic load. As the deformation of the soft surface increases, the cracks begin to nucleate below the surface, and further cyclic loading promotes the formation of cracks parallel to the surface. When the cracks finally extend to the surface, the thin wear sheets peel off and form flake debris, which eventually forms the depressed damage zone.

3.2.1. Factors of previous studies

The process of contact fatigue is very complex with many influencing factors, and it is difficult to make a decision by simple analysis. The factors affecting wheel/rail surface fatigue can be summarized as follows:

1. With the increase of normal load, the wear amount of wheel and rail and the friction factors in the rolling friction stability stage both increase, and the massive spalling and cracks on the surface also increase with the increase of normal load [27].

2. Main damage types of rail although their failure mechanisms are different, the main influencing factor is the surface friction between wheel and rail. With the increase of surface friction, all kinds of rail damage will be aggravated. Therefore, in the section with high surface friction, such as curve, ramp line, rail damage is aggravated [28].

3. The crack initiation point is limited to a narrow area, with a typical depth of 0.3mm, which is consistent with the position of the maximum shear stress. The strength criterion of contact fatigue is also expressed as the maximum shear stress criterion [29].

4. Sliding may be an important factor to increase fatigue damage. Uneven sliding distribution in the Hertz contact zone also contributes to increased stress development, which significantly shortens the expected fatigue life of steel [30].

5. As the slide-roll ratio increases, the surface damage of wheel-rail materials gradually develops into fatigue wear, accompanied by oxidation wear and abrasive wear. The degree of abrasive wear also increases with the increase of slide-roll ratio (damage behavior of wheel-rail materials under different slide-roll ratios) [31].

So many parameters have an important influence on the surface damage of rail, and they have a complex interaction with each other. In the case that the steel and wheel materials are fixed, but the surface state is always changing, the friction factor is always changing. Moreover, the research of article [31] also shows that: The initial value of friction coefficient is about 0.1, 0.2 and 0.3 with the increase of roll ratio under different roll ratio. Moreover, the friction factor of rolling friction is much smaller than that of

sliding friction. When wheel-rail relative sliding friction occurs, the high temperature caused by high friction will also change the hardness of materials and crystal structure to change the wear resistance of metal. The hardness of metal usually decreases with the increase of temperature, so sliding friction plays a more decisive role in rail damage than friction.

3.2.2. Factors of theoretical analysis

According to Hertz wheel-track contact theory, contact force is elliptic. Within the range of contact spots obtained according to normal clearance, it is assumed that the contact spots are about the face scale formed between axle and main contour line (the influence of shaking head Angle on contact spot shape is temporarily ignored) [32]. When the normal force N is known, the normal phase contact stress p_0 on the contact spot is:

$$p_0 = \frac{N}{\int_{-a}^{a}\int_{0}^{b_1}\sqrt{1-\frac{y^2}{b_1^2}}\sqrt{1-\frac{x^2}{a_f^2}}dxdy + \int_{-a}^{a}\int_{b_2}^{0}\sqrt{1-\frac{y^2}{b_2^2}}\sqrt{1-\frac{x^2}{a_f^2}}dxdy} \qquad (1)$$

The calculation of wheel-rail stress is complicated, but only the normal stress, shear stress and other factors are analyzed here, and the contact surface is simply approximated as a circular spot instead of an ellipse. So:

$$p_0 = \frac{N}{\pi a^2} \qquad (2)$$

When the contact area reaches the minimum and the load reaches the maximum, p_0 reaches the maximum value P_{max}. As an important parameter, the shear stress needs further analysis. Research in [33, 34] shows that the limit value of stability is greatly influenced by tangential force. Therefore, under the same normal load, with the increase of tangential force, the probability of plastic deformation of rail will increase rapidly. Therefore, in some sections of the line with high tangential force, such as the braking or starting section and the curve section, the rail's ability to resist plastic deformation will decrease rapidly, and the rail's collapsibility will increase rapidly.

The friction resistance under free rolling is small, and the friction coefficient at this time is only about one-tenth of the friction coefficient under controlled rolling when the braking distance is applied. Shear stress is the main cause of the permanent fatigue crack. With the increase of friction, the shear stress becomes larger and larger, and the peak shear stress is closer and closer to the surface. At this time, the micro crack expands in the deformation layer and the surface layer, and extends to the surface of the core rail, accompanied by the plastic deformation caused by the pressure exceeding the yield stress of the core rail. Under the action of repeated loads, the plastic deformation will accumulate and increase, and the cracks will continue to expand and form fish scale cracks distributed on the surface of the rail. If the rail surface crack is not dealt with in time, the surface crack will expand to the rail body along the direction of movement, and then the large strip. When the surface friction force increases to a certain value, the surface wear type changes, the surface is consistent with the direction of motion, there are obvious scratches, and there are also large flake flakes of wear debris, indicating that in addition to abrasive wear, there are obvious fatigue wear and adhesion wear. Rail stripping is mainly caused by the action of surface friction. With the increase of friction, the peeling phenomenon of material surface increases and the peeling chip block increases.

Shear stress is calculated according to Smith's contact stress theory as follows [35] :

$$\tau_{xz} = -\frac{P_{max}}{\pi}\left\{ z^2\psi_2 + \mu\left[(a^2 + 2x^2 + 2z^2)\frac{z}{a}\psi_1 - 2\pi\frac{z}{a} - 3xz\psi_2 \right]\right\} \tag{3}$$

where α is the half width of the contact surface; μ is the friction coefficient of the contact surface; $\psi1$, $\psi2$ is the derived coefficient, and its expression is as follows:

$$\psi_1 = \frac{\pi}{k_1} \cdot \frac{1 + \sqrt{k_2 / k_1}}{\sqrt{k_2 / k_1} \cdot \sqrt{2\sqrt{k_2 / k_1} + (k_1 + k_2 - 4a^2)/k_1}} \tag{4}$$

$$\psi_2 = \frac{\pi}{k_2} \cdot \frac{1 + \sqrt{k_1 / k_2}}{\sqrt{k_1 / k_2} \cdot \sqrt{2\sqrt{k_1 / k_2} + (k_1 + k_2 - 4a^2)/k_2}} \tag{5}$$

$$k_1 = (a + x)^2 + z^2; k_2 = (a - x)^2 + z^2 \tag{6}$$

Because the contact area size here is also very small, the calculation is simplified, then: $x = 0$, $k_1 = k_2$, $\psi_2 = 0$. By substituting the above formula into (3), the following formula can be obtained.

$$\tau_{xz} = -P_{max} \cdot \frac{\mu z}{\pi a}\left[(a^2 + 2z^2)\frac{\pi}{\sqrt{a^2 + z^2} \cdot z} - 2\pi \right] \tag{7}$$

According to the above formula, it is obvious that the forward pressure N and the contact area play a decisive role in the forward stress and tangential stress. The shear stress reaches its maximum when it is a certain depth away from the surface layer. Article [33] shows that this value is about 0.03 mm. It can be concluded that the positive pressure and the change of contact area play a decisive role in rail damage under fixed rolling conditions.

3.2.3. Lateral shift of wheel

Literature [36-39] comprehensively carried out a series of studies on wheel-rail rolling contact fatigue problems, popularized the results of Kalker's latest theory and developed Kalker's theory. The studies also show that the larger the transverse amount of rail will produce a larger shear stress and normal stress. Because of the wheel set left and right lateral movement of the rail produced when sliding friction contact [38]. Sliding contact method to contact force of wheel and rail and wheel under the condition of dynamic load and dynamic load coefficient is greater than the value of the rolling contact condition. Under the condition of sliding contact spot near the thermal stress is greater than the value of the rolling contact condition under the condition of sliding contact rail wear volume and the surface plastic strain is greater than the value of the rolling contact condition.

Contact fatigue crack is the main damage of rail under wheel/rail rolling contact. Abrasion is the main damage of rail under sliding contact. The maximum values of wheel-rail normal contact force and wheel dynamic load increase with the increase of axle load and sliding speed. The friction coefficient of rail increases with the increase of axle weight, sliding speed and wheel vibration frequency. Research [41] shows that when the wheelset traverse is -8~0 mm, the maximum contact stress increases first and then decreases due to the continuous fitting of the wheel rail tread, but the range of change is not large, and

the contact stress varies between 1500~2500 MPa. However, when the rate of traverse changes from 0 mm to 8 mm, the maximum contact stress firstly decreases and then increases sharply. This is because when the value of traverse changes from 0 mm to 4 mm, the wheel-rail profile is more matched and the contact spot area is larger. When the value of traverse continues to increase, the contact area decreases sharply due to the angular contact between wheel and rail gauge, resulting in a sharp increase in contact stress.

Although the outline of frog rail is not the same as that of steel rail, it can be predicted that the increase of lateral movement will inevitably lead to an instantaneous increase in stress. Because the result of computer simulation is the contact area of wheel-rail decreases instantly when there is a large amount of traverse, the stress of frog rail will increase even if the same force is applied. At this time the frog rail bears all the pressure from the wheel. Therefore, in this paper, the main parameters of damage of frog rail surface are soft wave, hard impact α, load, lateral displacement. The load is measured mainly from the vertical pressure, while the lateral displacement is mainly expressed as the change of the lateral wheel-rail force. The increase of lateral movement will obviously lead to the increase of roll ratio.

3.3. Major factors of frog rail failure

There are two special temporal and spatial nodes in the process of the wheel passing through the frog rail. When the wheel just touches the frog rail, it is prone to more and greater impact because of the direct collision between the wheel and the center rail in the forward direction. The other node directly acts on the frog rail when the wheel leaves the side rail completely, and the frog rail bears the entire load at this time. At the stage, before and after the wheel just contacts the frog rail, the wing rail contacts the wheel at the same time, and both sides jointly bear the load from the vehicle (Fig. 7). In the actual situation, due to the change of the wear conditions of the various components in the crossing area and the different lateral relative positions of the wheels entering the crossing, the two situations mentioned above may occur simultaneously within a small length space of the frog rail.
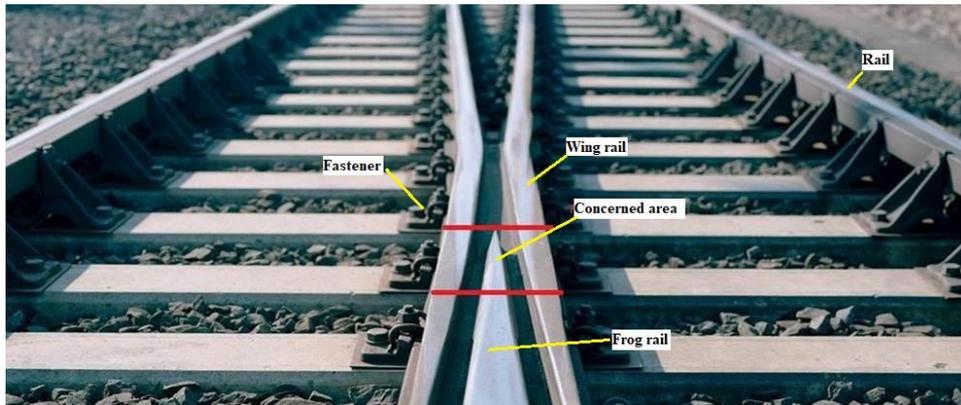
Fig. 7 The main study area of frog

Experimental measurements by Guo et al. [42] show that the surface hardness of frog rail and the depth of hardened layer are the highest in all seven positions of the crossing railhead segment with the cross-section surface width of 20 mm and 50 mm. This region is about 200

- 450 mm from the tip of frog rail, which is consistent with the simulation results in this paper. The wheel-rail contact stress with axle load of 21 t can reach more than 1230 MPa when it runs normally on the smooth track. Many of today's trains exceed that. Therefore, the stress of wheel-rail contact in the frog rail area must exceed the ultimate strength of the frog rail. As long as the wheel passes through the rail, it will inevitably cause damage to the rail. When the wheel travels from the tip of frog rail to the bottom end with a larger cross-section, the impact and load are obviously greater than the impact when the wheel travels from the bottom end to the tip. Therefore, this paper chooses the former as a case in the analysis. Generally, the area where the frog track and wheelset interact is transition zone.

3.3.1. Impact force

In the experiment of damage detection on frog rail, conducted in 2019 [18], the distribution of the impact load borne by the frog rail in the longitudinal area of the frog rail is obtained. The research and analysis showed that the rail surface is subjected to higher frequency impact when the wheel entered the rail tip. As shown in Fig. 8, in the 1:12 crossing, 70 % of the shocks are concentrated in the 220 - 320 mm area, of which the transverse and longitudinal shocks are mainly concentrated in 50 g or less shocks. These are common in normal sections, while the vertical shocks are even as high as 300 g and most of the shocks are concentrated in 130 - 240 g. The study estimates the influence of one impact with an acceleration of more than 250 g to be equivalent to more than one thousand impacts of 50 g. Relevant results have been shown in detail in paper [18]. This region is the main impact region, which bears most of the wheel-rail impact during the whole life process.

The wing rails in this area bear part of the vehicle's pressure, so if the first damage occurs in this area, it is due to the high frequency of vertical impact load. Therefore, it is necessary to understand the action mechanism of impact load. Shi imposes a heavy impact load on hard aluminum alloy, to observe the damage behavior of the hard aluminum alloy. The test results show that the heat generated by the heavy impact passes around, making the bulge deformation. The impact on the part of the subtle grain broken flower, increased with the increase of load and the number of times, increasing the impact will micro cracks appear and expand [43]. In their paper [44], Hu et al. conducted an experimental study on the wear characteristics of high-hardness steel dies under shock loading conditions. Under the action of impact stress and frictional stress, the grinding surface has micro-roughness, interlocking, and continuous slight sliding friction, which makes the surface layer highly, localized damage. As the number of impacts increases, the damage accumulates and microscopic plastic deformation occurs on the local surface. The stress concentration on the grain boundary or the phase interface leads to the generation of friction cracks, which continue to expand, and eventually lead to friction cracks and damage to the surface of the steel mold.

However, in the crossing area, the relative position of wheel and frog rail is normal distribution random position, and the change of speed and vibration will affect the impact position of load on frog rail. Therefore, each impact load of wheel on frog rail acts on a certain area but distributes at different drop points. The experiment of impact load on a variety of hard metals can be concluded that impact load will cause the deformation of frog rail surface, and there will be large wear and crack generation under long term impact action. A predictable conclusion can be drawn from the distribution points, experimental results that deformation, and crack are most likely to occur on the surface. Instantaneous impact and Hard Impact alpha are mainly caused by wear and cracks rather than the direct cause of peeling damage.
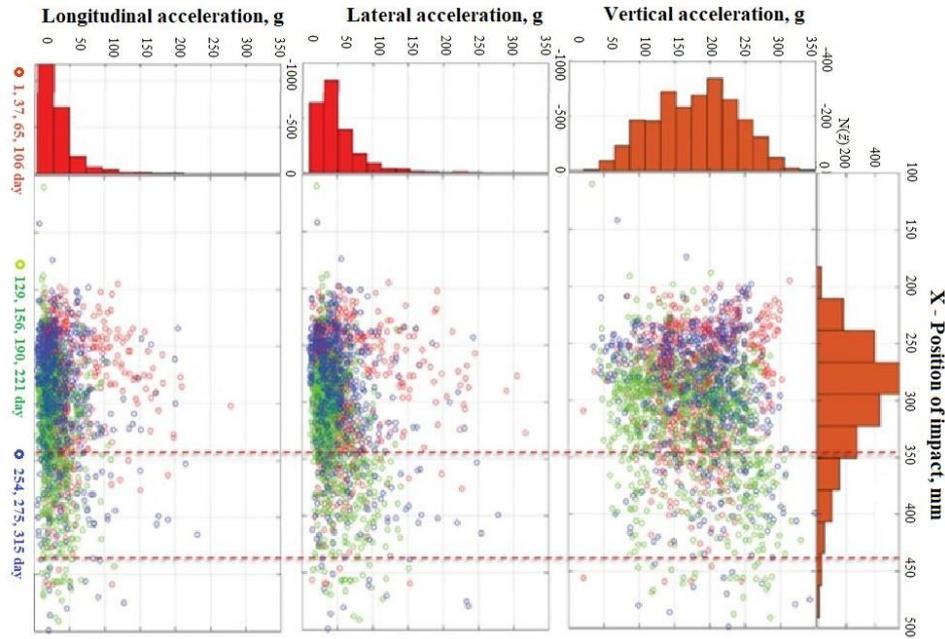
Fig. 8 The distributions of the longitudinal coordinates of the impact and of the corresponding maximal vertical accelerations for the frog rail of a common crossing [18]

3.3.2. Load and lateral movement

First, as the falling depth Z_S of the soft wave increases, the load acting on the frog rail will also increase. This is an obvious factor. Another position that may cause greater wear is in the section where the wheel leaves the wing rail and fully acts on the frog rail, considering the normal wheel width is 135 mm to 140 mm, S_d is 32.5 mm. The wheel has a certain lateral movement range, the maximum is 11.5 mm the maximum probability according to the normal distribution law of the experimental statistics is 4 - 6 mm. The distance between the wing rail and the frog rail is a discrete point with normal distribution. When the wheel completely leaves the wing rail and falls on the frog rail, the surface of the wing rail has a drop of 1-2mm compared with the frog rail. At this time, the train is still moving forward. After the wheel completely leaves the wing rail and advances a short distance, it falls within the range of about 330 - 430 mm on the surface of the frog rail (as shown in Fig. 9).

Now before the wheel completely falls on the frog rail, the shape of the outer part of the wheel and the outer part of the wing rail as shown in the figure leads to the inward extrusion of the rail on the wheel, resulting in a large amount of transverse movement of the wheel at this time. When the wheel falls on the frog rail and moves inward, it will hit the guardrail, and the collision with the guardrail will make the wheel move outward. Therefore, within that range the wheels are going to be moving sideways a lot. The wheel and the frog track slide in the lateral direction. Ren and Wan study in [45, 46] have confirmed the above conclusion. The vehicle-rail space model and coupling with vibration constructed by the team analyzes the vibration characteristics of the vehicle through the

crossing system. The results show that the lateral acceleration response of the train will be larger. When the wheels enter the crossing and leave the wing rail, but the latter is especially obvious at 1.83 m/s^2. The specific action process is that the wheelset moves toward the inner rail due to lateral extrusion when it breaks away from the side rail, but under the action of the guide curve, it quickly moves toward the outer gauge and reaches the maximum lateral movement. According to the team's simulation data, it can be moved inwards by as much as 6 mm in an instant and outwards by as much as 11 mm again. In order to verify this view, the research team also measured the lateral acceleration of frog rail along the traveling direction, which was consistent with the theoretical results. Relevant research has been described in paper [18].
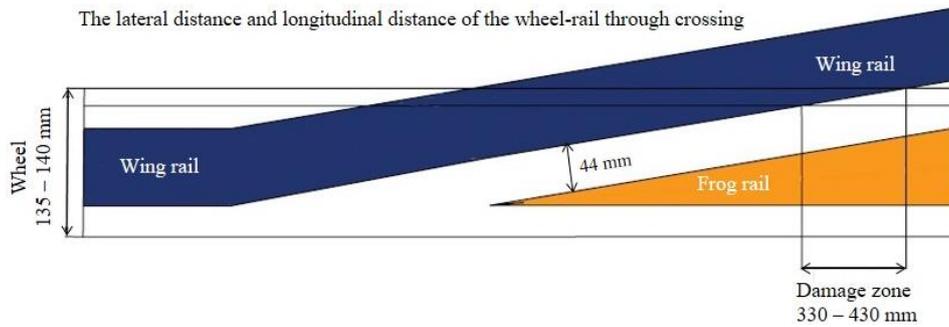
Fig. 9 Distance of leaving the wing rail area

In this area, a portion of the wheel starts to be fixed in a small area where impact and wheel traverse occur. The generation and development of wheel-rail rolling contact fatigue depend on the normal force and tangential (creep) force on the contact spot. The sliding friction and lateral force generated by transverse movement will inevitably lead to the decrease of the wheel-rail contact area and the increase of the normal and tangential force, reaching the maximum value. Therefore, this paper considers that the probability of surface stripping in the departure area of the frog rail is far greater than that in other areas, and surface stripping will aggravate the wear of the frog rail and cause more serious damage. Therefore, the region where sufficient lateral displacement occurs in the fixed frog rail is the largest damage area. At the same time, it needs to be simulated to check whether the depth of the soft wave in this area will also increase

4. RESULTS

According to cast high manganese steel frog minor damaged criteria, at the cross section of frog rail width 40 mm, the frog rail wears vertically (excluding the heightened part of wing rail);

Rails of 50 kg/m and below: exceed than 4 mm on the main line, exceed than 6 mm on the branch line, and exceed than 8 mm on other lines;

Rails of 60 kg/m and above: exceed 4 mm on the main line with an allowable speed greater than 120 km/h, exceed 6 mm on other main lines, exceed 8 mm on branch lines, and exceed 10 mm on other lines.

In this paper, several models are used to simulate the evolution process of contact points when the vertical wear of the frog rail is from 0 to 5 mm. The position between the touchdown point and the tip of the frog rail when the wheel touches the frog rail for the first time and when the wheel leaves the wing rail is recorded respectively.

In order to be able to determine the touchdown point, two further parameters (wave depth Z_s and touchdown angle α) must be calculated. First, the wheel trajectory should be preserved, because the wheel is not a regular plane, but an area with a slope and curvature. Therefore, the size of the wheel trajectory cannot be determined based on the value of the contact points. The line connecting the minimum distance of each section is actually the wheel trajectory on the plane formed by the X- and Z- axes, but its shape varies, since the wear of the frog changes the geometry during the service life.

The stimulation soft wave depth Z_S and the contact angle α were calculated from the wheel trajectory as Fig. 10 presents them. Here only the range from x = 0 mm to x = 500 mm is selected for the calculation. The wave depth could be clearly identified, but the angle of contact α can be calculated.
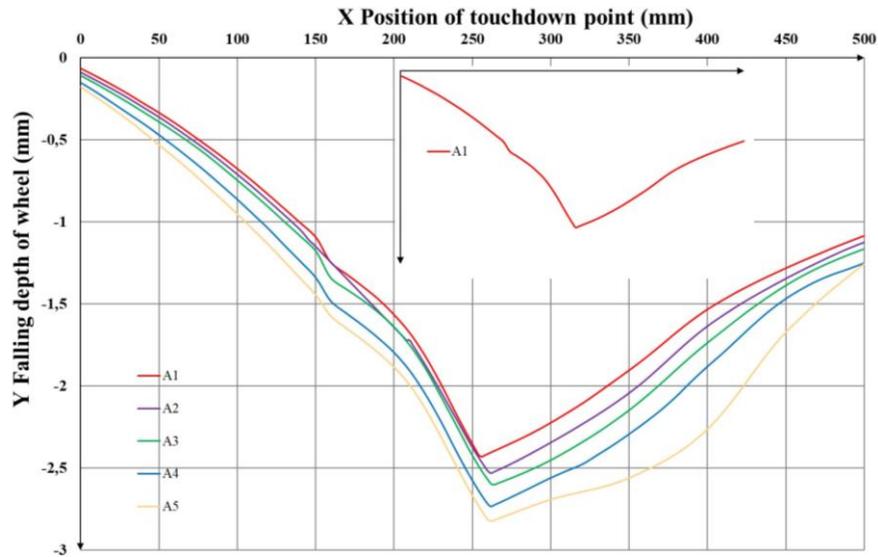

Fig. 10 Change of impact angle and wave depth

As the accumulated traffic mass increases, the angle of touchdown becomes smaller, but the depth of the shaft increases. We know that the touch down angle α stands for hard impact and the wave depth Z_S for soft impact. By changing these two parameters, one can speculate with the increase in the accumulated traffic mass about the changes in the loads on the crossinges. The impact angle and touch down point of the frog appear within a certain range, and the wave depth keeps increasing. For a frog, the X_{TP} of the touch point does not always increase, but only fluctuates within an area. The wheel trajectory is also significantly different due to wear. The reason is that the wear of the wing rail is not considered in advance. If we only use geometry data that does not consider wing rail wear, the frog tip will continue to wear over time. Therefore, a geometric model of the control variable is required.

Then simulated (in Fig. 11) the change of position of touchdown point respectively in abrasion of the wheel at 0.5 mm and 1 mm and also with the frog rail abrasion. Fig. 11 (a) shows where the wheel begins to contact the frog rail. Fig. 11 (b) shows the position where the wheel is completely disengaged from the wing rail. With the frog rail wearing, the positions of the touchdown point points are significantly away from the frog rail tip. When the vertical wear is reached the slight injury standard, the distance has exceeded 330 mm. In this range, the track gauge wheel leaves the wing rail in advance. A certain number of wheels have had multiple impacts on a small range. With the increase in frog rail wear, this situation will become more serious. The wheel wear also has a significant impact on the movement of the touchdown point. With the increase in wheel wear, the touchdown point also moves back significantly. In order to understand the influence of wing rail wear on contact point change, the wing rail wear of 0.5 mm and 1 mm is simulated (Fig. 12). Although the wear of the wing rail prevents the backward movement of the touchdown point, the improvement effect is not obvious.
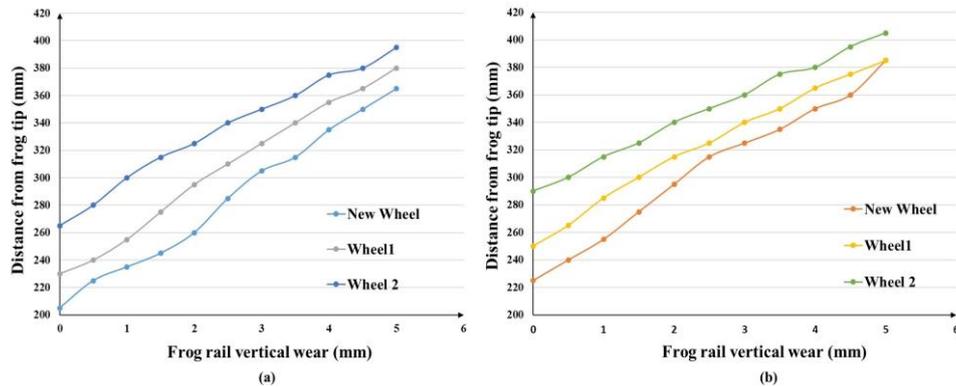
**Fig. 11** Changes in contact points after wheel wear
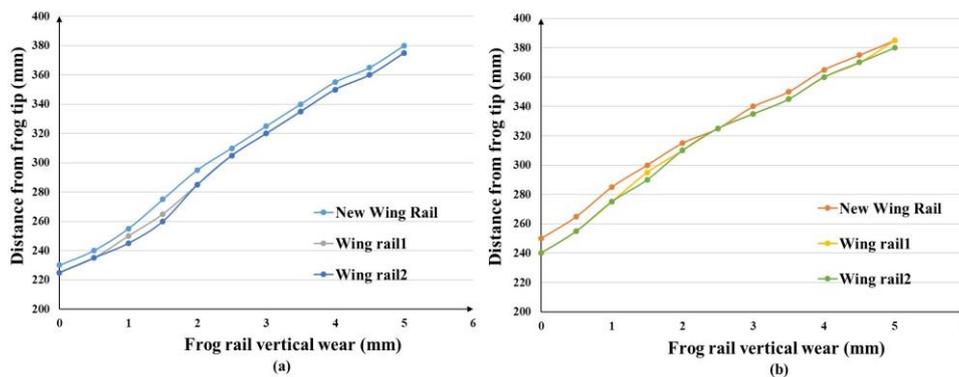
Fig.12 Changes in contact points after wing rail wear

The research results obtained in article [47, 48] can prove that when the contact point moves backward, the frog rail is subjected to greater and greater impact load. In the end of frog

rail, the frog rail is worn with the increase of impact, and then the impact point moves backward. When the backward moving area reaches 350 mm, the vertical impact force increases. Some wheels have been in the stage of only acting on frog rail in this area, constantly influencing in a fixed area and generating huge load. This situation increases with the backward movement of the contact point, the impact increases, and the transverse movement will increase, causing peeling and other damage to the frog rail surface. Because the impact area is relatively fixed, the small spalling expands to the damage of complete damage to the frog rail.

When the wheel reaches the area away from the wing rail, even if the wear changes, some wheels with a large distance from the frog rail will not move back. With the increase of wear, the contact point moves back, and the effect of more wheels on the frog rail surface is concentrated in a certain area. As the wave depth increases, the frog rail load increases accordingly. Stronger impact and greater lateral movement are concentrated in this area. Moreover, it will not move due to the increase of wear. Repeated action, even without too high frequency, will quickly lead to the peeling and damage of frog rail surface based on existing wear. In order to verify the correctness of the analysis, Jianxing Liu collected 25 frog rail surface damage images in different wear periods in China, sorted them into data, and measured and counted the location of maximum surface damage of frog rail, as shown in Fig. 13.
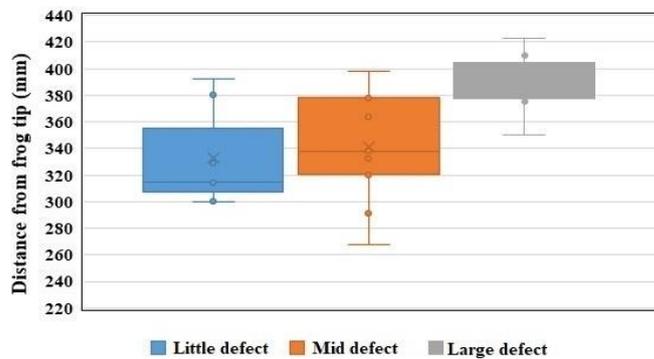
Fig. 13 Location of maximum surface damage of frog rail

Although the maximum damage area of simulation and measurement results is concentrated in the 6cm area of 350 - 410 mm, the sampling and simulation data are very limited. As the allowable error, we define this range as 10cm, i.e. 330 - 430 mm. For computer vision inspection, only one sampling is needed to obtain the photos that can see the micro cracks best. The above measured results verify the accuracy of this study. Although the 230 - 330 mm area considered by the traditional view will also produce surface damage in the early stage, it has been proved that the maximum damage position occurs after the wheel leaves the wing rail and moves laterally. With the wear of frog rail and wheel, the location of the maximum damage is concentrated in the range of 350 mm to 420 mm. Because the geometric model cannot consider the vehicle body shaking and tilting and the lack of corresponding mechanical feedback data, there must be some errors. However, the results of data feedback from real measurement are completely consistent with the results of theoretical analysis. This study shows that properly reducing the height of wing rail can slow down the backward movement of contact point, reduce the impact of the wheel on the center rail so as to prolong the service life of crossing.

5. Conclusions

The surface damage detection of frog rail is always a complicated problem, and the main cause of its damage formation has not been determined yet. In this paper, the contact process of wheel passing frog rail is calculated by establishing geometric model. The changes of contact points with increasing wear of wheel, wing rail and frog rail were simulated and the main contact area was established. Through literature research and summary, the main parameters of rail damage are determined. Through further theoretical analysis, we find the main areas where the maximum damage may occur with the increase of service life of frog rail surface. The following conclusions can be drawn:

1. The forces acting on the frog are mainly caused by two factors: wave excitation and impact excitation. The resulting wave excitation and impact excitation creates loads when the wheel passes the point facing or vice versa.The train speed and wave depth affect the value of the soft impact. The size of the hard impact is affected by the speed and the angle of touchdown.

2. The larger the area of the touchdown distribution, the longer the service life of the common crossing. The position of the touchdown point will change by changing the position of the wheel set in the track gauge. The elastic vertical deformation of the frog also influences the position of the touchdown point. As can be seen from the trends of the parameters, the soft impact grows with raising of the accumulated traffic mass, on the contrary, the hard impact becomes smaller.

3. Vehicle load, friction coefficient, slip roll ratio and shear stress are the main factors affecting the service life of the track. Their increase accelerates rail fatigue damage.

4. When the material is fixed, the load and wheel lateral movement are the most important factors causing the damage of frog rail surface. Lateral movement mainly reduces the contact area and sharply increases the tangential stress.

5. Wheel wear and vertical wear of frog rail will lead to the acceleration of backward movement of contact point, the increase of wheel rail force and the damage of frog rail surface. The vertical wear of wing rail is beneficial to prolong the service life of frog rail.

6. In the area where the wheel geometry cannot act on the frog rail and wing rail at the same time, with the increase of wear, this area will produce concentrated wheel rail contact, causing rapid damage to the frog rail surface.

7. The maximum damage area of frog track is determined at the 1:12 fixed frog crossing 330 mm to 430 mm from the vertex, and the traditional 200 - 500 mm area is reduced by 60 %. The time loss and cost of testing are greatly reduced.

At the same time, the method has universality and can be extended to any type of crossing damage research. Of course, this paper also has some limitations, crossing wear simulation and reality are not completely consistent, for the exact force is not fully understood, and these problems will be further completed in the follow-up study. The research results in this paper have good practical application value and lay a foundation for the future research on frog tunnel surface damage identification and damage development prediction.

REFERENCES

1. Szalai, S., Eller, B., Juhász, E., Movahedi, M.R., Németh, A., Harrach, D., Baranyai, G., Fischer, S., 2022, *Investigation of deformations of ballasted railway track during collapse using the Digital Image Correlation Method (DICM)*, Reports in Mechanical Engineering, 3(1), pp. 258-282.
2. Plášek, O., Raif, L., Vukušic, I., Salajka, V., Zelenka, J., 2019, *Design of new generation of switches and crossings*, Future Trends in Civil Engineering 2019, pp. 278-301.
3. Macura, D., Laketić, M., Pamučar, D., Marinković, D., 2022, *Risk Analysis Model with Interval Type-2 Fuzzy FMEA – Case Study of Railway Infrastructure Projects in the Republic of Serbia*, Acta Polytechnica Hungarica, 19(3), pp. 103-118.
4. Izvoltova, J., Ižvolt, L., Šestáková, J., 2021, *Analysis of Methods Used to Diagnostics of Railway Lines*, in: de Luca, S., Di Pace, R., Fiori, C. (Eds.), *Railway Transport Planning and Management*, doi: 10.5772/intechopen.100835
5. Utrata, D., Clark, R., 2003, *Groundwork for Rail Flaw Detection Using Ultrasonic Phased Array Inspection*, Review of Quantitative Nondestructive Evaluation, 22(1), pp. 799-805.
6. Papaelias, M.P., Lugg, M.C., Roberts, C., Davis, C.L., 2009, *High-speed Inspection of Rails Using ACFM Techniques*, NDT & E International, 42(4), pp. 328-335.
7. Kou, L., 2022, *A Review of Research on Detection and Evaluation of the Rail Surface Defects*, Acta Polytechnica Hungarica, 19(3), pp. 167-186.
8. Marino, F., Distante, A., Mazzeo, P.L., Stella, E., 2007, *A Real-time Visual Inspection System for Railway Maintenance: Automatic Hexagonal-headed Bolts Detection*, IEEE Transactions on Systems Man& Cybernetics-Part C: Applications & Reviews, 37(3), pp. 418-428.
9. Xu, J.M., Gao, Y., Wang, P., An, B.Y., Chen, J.Y., Chen, R., 2020, *Numerical analysis for investigating wheel-rail impact contact in a flange bearing frog crossing*, Wear, 450–451(2), 203253.
10. Tigh Kuchak A.J., Marinkovic D., Zehn M., 2020, *Finite element model updating - Case study of a rail damper*, Structural Engineering and Mechanics, 73(1), pp. 27-35.
11. Cao, Y., Zhao, W.H., Lin, Y.R., Yao, K.J., Lin, X.R., 2020, *Dynamic optimization of the rail-crown geometry in the rigid frog area by controlling the position of the wheel-load transition*, Proc IMechE Part F: J Rail and Rapid Transit, 234(9), pp. 1017–1028.
12. Khoshravan, M.R., Khadivi, O., Paykani, A., 2013, *Finite Element Analysis and Experimental Study of Stress Distribution in Straight Frog of Railway Needle*, Journal of Failure Analysis and Prevention, 13(1), pp. 72–79.
13. Kovalchuk, V.V., Sysyn, M.P., Sobolevska, Y.H., Nabochenko, O., Parneta, B., Pentsak, A., 2018, *Theoretical Study into Efficiency of the Improved Longitudinal Profile of Frogs at Railroad Switches*, Eastern-European Journal of Enterprise Technologies, 4(1), pp. 27-36.
14. Kuchak A.J.T., Marinkovic D., Zehn M., 2021, *Parametric Investigation of a Rail Damper Design Based on a Lab-Scaled Model*, Journal of Vibration Engineering and Technologies, 9(1), pp. 51–60.
15. Ma, H., Zhang, J.M., Zhang, J., Jin, T.T., Song, C.Y., 2020, *Influence of Full-Life Cycle Wheel Profile on the Contact Performance of Wheel and Standard Fixed Frog in Heavy Haul Railway*, Shock and Vibration, 2020, 8866692.
16. Kuminek, T., Aniołek, K., Młyńczak, J., 2015, *A numerical analysis of the contact stress distribution and physical modelling of abrasive wear in the tram wheel-frog system*, Wear, 328–329, pp. 177-185.
17. Sysyn, M.P., Gerber, U., Nabochenko, O., Gruen, D., Kluge, F., 2019, *Prediction of Rail Contact Fatigue on Crossings Using ImageProcessing and Machine Learning Methods*, Urban Rail Transit. 5(2), pp. 123-132.
18. Sysyn, M.P., Kluge, F., Gruen, D., Kovalchuk, V.V., Nabochenko, O., 2019, *Experimental Analysis of Rail Contact Fatigue Damage on Frog Rail of Fixed Common Crossing 1:12*, Journal of Failure Analysis and Prevention, 19(21), pp. 1077-1092.
19. Xin, L., Markine, V.L., Shevtsov, I.Y., 2016, *Numerical procedure for fatigue life prediction for railway crossing crossings using explicit finite element approach*, Wear, 366-367, pp. 167-179.
20. Yang, X.W., Zhang, Z., Meng, W., Qian, D.W., Hu, Y.H., 2020, *Effect of Vertical Wear of Unmovable Frog Nose Rail on Dynamical Wheel-Rail Contact in Crossing Zone*, Journal of Tongji University, 48(11), pp. 1595-1604.
21. Aniołek, K., Herian, J., 2013, *Numerical Modeling of Load and Stress on the Contact Surface of a Crossing and a Railway Vehicle*. Journal of Transportation Engineering, 139, pp. 533-539.
22. Nielsen, J.C.O., Palsson, B.A., Torstensson, P.T., 2016, *Crossing Panel Design Based on Simulation of Accumulated Rail Damage in a Railway Crossing*, Wear, 366-367, pp. 241-248.
23. Ashtiani, I.H., 2017, *Optimization of secondary suspension of three-piece bogie with bevelled friction wedge geometry*, International Journal of Rail Transportation, 5(4), pp. 213–228.

24. Kaiser, I., Poll, G., Voss, G., Vinolas, J., 2019, *The impact of structural flexibilities of wheelsets and rails on the hunting behaviour of a railway vehicle*, International Journal of Vehicle Mechanics and Mobility, 57(4), pp. 564–594.

25. Fengler, W., Gerber, U., 2007, *Loading of common crossings. (GER: Belastung von Weichen mit starrer Herzstueckspitze)*, ZEVrail Glas. Ann., 2007(5), pp. 202–214.

26. Plasek, O., Hruzikova, M., 2017, *Under sleeper pads in switches & crossings*, IOP Conference Series Materials Science and Engineering, 236(1), 012045.

27. Huang, J., Zhou, Z., Peng, J.F., Cai, Z.B., Jin, X.S., Zhu, M.H., 2016, *Rolling Friction and Wear, and Damage Behavior of Wheel/Rail at High Rotation Speed and Different Normal Loads.* Meterials for Mechanical Engineering, 40(6), pp. 88-92.

28. Liu, Q.Y., Zhang, B., Zhou Z.R., 2002, *Research on damage mechanism of railway rail*, China Mechanical Engineering, 18(13), pp. 1596-1599.

29. Wen, S.Z., Huang, P., 2002, *Tribological Principle.* Tsinghua University Press, pp. 327-330.

30. Fourel, L, Noyel, J.P., Bossy, E., Kleber, X., Sainsot, P., Ville, F., 2021, *Towards a grain-scale modelling of crack initiation in rolling contact fatigue - Part 2: Persistent slip band modelling*, Tribology International. 163, pp. 107173.

31. Zhou, Y., Peng, J.F., Zhao, L., Wang, W.J., Li, W., Jin, X.S., Zhu, M.H., 2016, *Damage Behavior of Wheel/Rail Materials under Different Slip Rates*, Journal of Materials Engineering, 44(2), pp. 75-80.

32. Kalker J.J., 1990, *Three Dimensional Elastic Bodies in Rolling Contact*, Boston: Kluwer Academic Publisher, pp. 20-101.

33. Ekberg, A., Kabo, E., Andersson, H., 2002, *An engineering model for prediction of rolling contact fatigue of railway wheels*, 25(10), pp. 899-909.

34. Kabo, E., Ekberg, A., Torstensson, P.T., 2010, *Rolling contact fatigue prediction for rails and comparisons with test rig results*, Proceedings of the Institution of Mechanical Engineers–Part F：Journal of Rail and Rapid Transit, 224(4), pp. 303-317.

35. Sheng, G.M., Fan, J.H., Peng, X.H., 2000, *Investigation of contact fatigue crack growth behaviors for PD3 rail steel*, Acta Metallurgica sinica, 36(2), pp.131-134.

36. Santamaria, J., Vadillo, E.G., Gomez, J., 2006, *A Comprehensive Method for the Elastic Calculation of the Two point Wheel/Rail Contact*, Vehicle System Dynamics, 44(5), pp. 240-250.

37. Jin, X.S., Liu, Q.Y., 2004, *Wheel and rail rubbing*, Beijing: China Railway Publishing Club, pp. 105-107.

38. Jin, X.S., Wen, Z.F., Zhang, W.H., 2004, *Analysis of wheel-rail rolling contact stress of two profiles*, Chinese journal of mechanical engineering, 40(2), pp. 5-10.

39. Tao G.Q., Li X., Wen Z.F., Jin, X.S., 2013, *Comparative analysis of two wheel-rail contact stress algorithms*, Engineering mechanics, 30(8), pp. 229-235.

40. Jin X.S., Wen Z.F., Zhang W.H., 2004, *Effect of wheelset motions on the rolling contact stresses of wheel and rail*, Chinese journal of mechanical engineering, 21(1), pp. 165-172.

41. Yang, X.W., Zhao, Y.M., Zhou, S.H., 2017, *Calculation of Influencing Number of Wheel-Rail Non-Hertz Contact Using Finite Element Method*, Journal of Tongji University, 45(10), pp. 1476-1482.

42. Guo, S.L., Sun, D.Y., Zhang, F.C., Feng, X.Y., Qian, L.H., 2013, *Damage of a Hadfield steel crossing due to wheel rolling impact passages*, Wear, 305(30), pp. 267-273.

43. Shi, C.X., Wang, J., Chen, F.X., Li, H.S., 2011, *Wear of duralumin in under heavy impact load*, Lubrication and sealing, 36(2), pp. 38-44.

44. Hu, Z.H., Yang, X.C., 1989, *Wear characteristics and influencing factors of high hardness die steel under impact loading*, Materials for Mechanical Engineering, 13(4), pp. 51-55.

45. Ren, Z.S., Zhai, W.M., Wang, Qichang, 2001, *The use of spatial wheel/rail contact geometric relationship in the crossing system dynamics*, Journal of the China railway society, 23(5), pp. 11-15.

46. Ren, Z.S., Zhai, W.M., Wang, Qichang, 2000, *Study on lateral dynamic characteristics of vehicle crossing system*, Journal of the China railway society, 22(8), pp. 28-33.

47. Kovalchuk, V.V., Sysyn, M.P., Gerber, U., Nabochenko, O., Zarour, J., Dehne, S., 2019, *Experimental investigation of the influence of train velocity and travel direction on the dynamic behavior of stiff common crossings*, Architecture and Civil Engineering, 17(3), pp. 345-356.

48. Sysyn, M.P., Gerber, U., Gruen, D., Nabochenko, O., Kovalchuk, V.V., 2019, *Modelling and vehicle based measurements of ballast settlements under the common crossing*, European Transport, 71(5), pp. 1-25.